
This is an electronic reprint of the original article.
This reprint may differ from the original in pagination and typographic detail.

Shevchenko, Andriy; Setälä, Tero

Interference and polarization beating of independent arbitrarily polarized polychromatic optical waves

Published in:
Physical Review A


DOI:
[10.1103/PhysRevA.100.023842](https://doi.org/10.1103/PhysRevA.100.023842)

Published: 26/08/2019

Document Version
Publisher's PDF, also known as Version of record

Please cite the original version:
Shevchenko, A., & Setälä, T. (2019). Interference and polarization beating of independent arbitrarily polarized polychromatic optical waves. *Physical Review A*, 100(2), 1-7. Article 023842.
<https://doi.org/10.1103/PhysRevA.100.023842>

Interference and polarization beating of independent arbitrarily polarized polychromatic optical waves

Andriy Shevchenko ^{*}*Department of Applied Physics, Aalto University, P.O. Box 13500, FI-00076 Aalto, Finland*

Tero Setälä

Institute of Photonics, University of Eastern Finland, P.O. Box 111, FI-80101 Joensuu, Finland

(Received 4 June 2019; published 26 August 2019)

We study the properties of optical fields created by interfering polychromatic stationary waves that have different spectra and polarizations. Such fields can exhibit both deterministic and random intensity and polarization beatings, where the latter stands for a periodic variation of the field polarization state. For visible light, the beating period enters the femtosecond scale already when the central wavelengths of the waves differ by 10 nm. If the bandwidth of at least one of the waves is also on the order of 10 nm, the periodic variations are accompanied by ultrafast random changes which cannot be measured directly. We propose a set of statistical characteristics for such rapidly varying vector fields and practical methods to determine them in terms of fully time-averaged quantities. Our results may have impact on a variety of fundamental and applied aspects of optical polarimetry and interferometry.

DOI: [10.1103/PhysRevA.100.023842](https://doi.org/10.1103/PhysRevA.100.023842)

I. INTRODUCTION

Interference of optical waves is usually referred to as a phenomenon of periodic spatial modulation of light intensity in the region where the waves overlap. If the waves have the same central frequencies and mutually correlate, the modulation pattern stays fixed in space and time. If the waves do not fully correlate, the pattern fluctuates, which is observed as a decrease of its time-averaged visibility [1]. The area of applications of the interference phenomenon is wide, ranging from sensors of picometer-amplitude vibrations [2] to detection of cosmic gravitational waves [3]. Many important scientific and technological applications of optical interferometry are found in optical communication and information processing [4,5], laser cavity designs [6,7], correlation-based imaging [8–10], spectroscopy [11,12], and metrology [13].

In general, interfering electromagnetic fields can have different central frequencies and polarizations, and even be partially polarized. Interference in such cases has not previously been considered in much detail. Generalization of optical interferometry towards these cases may lead to discovery of new phenomena and development of new optical applications. For example, it has recently been demonstrated interferometrically that two fields with equal average intensities and degrees of polarization can have completely different dynamics of their instantaneous intensity and polarization state [14]. This fact can be used to extract additional information about the field source and propagation medium. Furthermore, significant progress has been recently achieved in structuring the polarization state of optical beams [15–19]. As an example, it has been shown that interference of an optical wave

with its orthogonally polarized frequency-shifted copy, such as its second harmonic, can result in complex polarization Lissajous curves instead of polarization ellipses and form optical beams with fractional-order angular momenta [15]. Such beams, as well as other optical fields with designed two- and three-dimensional polarization profiles [16–19], can show a variety of new spatially distributed dynamic polarization and interference effects.

In addition to ordinary electric-field interference, optical waves can show intensity interference based on correlations of the time-varying intensities of the waves. The intensity interferometry is a relatively new technique that can open up an additional dimension for optical investigations and applications. The technique has recently been used to characterize photon bunching in thermal light [20] and ultrafast polarization-fluctuation dynamics of polychromatic optical fields [14]. For intensity interferometry to be as sensitive as optical field interferometry, the intensity should fluctuate or be modulated fast and with a maximum modulation depth, which can be achieved, for example, by using wave beating [4]. This phenomenon is a result of interference of optical waves with the same polarizations, but different frequencies. It is applied, e.g., in heterodyne-type detection and sensing [4,21], optical velocimetry [22], optical frequency stabilization [23,24], and laser mode locking [6].

If the interfering waves are polychromatic and have not only different frequencies, but also different polarizations, the total field exhibits both periodic and random changes of its polarization state [14,25]. These effects have not been studied much, especially experimentally, because the variations are typically too fast to be directly measurable even by ultrafast photodetectors [14,26].

In this work, we consider such interfering polychromatic waves and address the possibility to measure their statistical

^{*}andriy.shevchenko@aalto.fi

properties. We show that, in general, the time-varying intensity and polarization of the total field can be represented in the Poincaré space by randomized elliptical trajectories of the end of the Poincaré vector. On average, these trajectories form a stretched torus. Therefore, to statistically characterize the behavior of the total field, the orientation and the thickness of the torus should be determined. We propose a practical way of doing this. Furthermore, we introduce a quantity, the beating harmonicity time, that is the time interval of a nearly periodic, predictable beating. This quantity depends on spectral properties of the interfering fields. The harmonicity time and other field characteristics introduced in this work can be measured in terms of time-averaged intensity correlation functions using intensity interferometry with slow photodetectors. The results of this work are applicable to various types of optical fields and may find applications in optical interferometry, polarimetry, and other related subdivisions of optics and photonics.

II. INTENSITY AND POLARIZATION BEATING OF MONOCHROMATIC BEAMS

Superposition of two monochromatic Gaussian beams with equal frequencies and polarizations that propagate in different directions (given by their wave vectors \mathbf{k}_1 and \mathbf{k}_2) yields a two-dimensional instantaneous interference pattern shown in Fig. 1(a). The field maxima move in the z direction (along $\mathbf{k}_1/k_1 + \mathbf{k}_2/k_2$) faster than light. Along the transverse x direction, they form a motionless standing wave that can be observed on a screen in the form of time-averaged, static interference fringes.

If the frequencies of the waves are different, the interference pattern acquires an asymmetry, as shown in Fig. 1(b). The maxima still move in the z direction, leading to a relatively slow shifting of the transverse fringe pattern on the screen along the x direction. The fringe period Λ_x is obtained from the x components of \mathbf{k}_1 and \mathbf{k}_2 using the equation $k_{1x}\Lambda_x = -k_{2x}\Lambda_x + 2\pi$. This yields

$$\Lambda_x = \frac{2\pi}{k_{1x} + k_{2x}}. \quad (1)$$

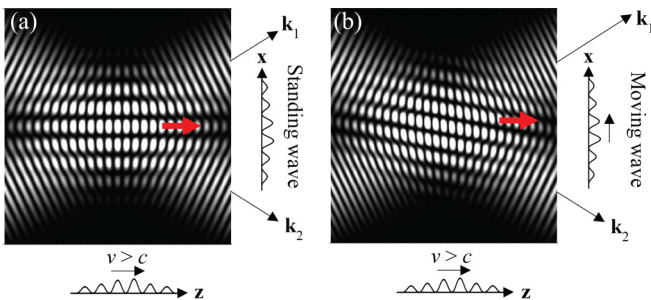


FIG. 1. Interference of monochromatic optical beams with (a) equal and (b) different frequencies. In (a), the interference fringes are perpendicular to the direction of motion of the pattern, while in (b) they are tilted, leading to temporal modulation of intensity at each point. In (b), if \mathbf{k}_1 and \mathbf{k}_2 are codirected, the fringes are wide and perpendicular to \mathbf{k}_1 and \mathbf{k}_2 .

When the fringes move, the waves have equal phases at a moving coordinate x , for which $k_{1x}x - \omega_1 t = -k_{2x}x - \omega_2 t$. This equation gives $2\pi x = (\omega_1 - \omega_2)\Lambda_x t$. During the beating period (T_b), the fringes move over a distance Λ_x in the positive x direction, if $\omega_1 > \omega_2$, which gives

$$T_b = \frac{2\pi}{\omega_1 - \omega_2}. \quad (2)$$

In general, the interfering waves can differ also in their polarizations, in which case the polarization state of the total field periodically varies in time. We call this variation *polarization beating* to contrast it to the former intensity beating [14,25]. Furthermore, in experiments, the interfering fields will necessarily be polychromatic, which for the case of different central frequencies makes the intensity and polarization beatings fluctuate.

III. BEATING HARMONICITY TIME

The intensity and polarization beatings can be considered predictable (essentially periodic) only within a finite time interval, τ_{bh} , that we call the *beating harmonicity time*. The intensity oscillation of the beating field after τ_{bh} cannot be predicted from the behavior of the original-field intensity, because the intensity variations separated by such time intervals do not correlate. For interference of statistically independent scalar (or equally polarized) waves, the correlation function of the intensity variations

$$M(\tau) = \langle \Delta I(t) \Delta I(t + \tau) \rangle = \langle I(t)I(t + \tau) \rangle - \langle I(t) \rangle^2, \quad (3)$$

where the angle brackets indicate time average, must decrease considerably at $\tau = \tau_{bh}$. If the waves have different polarizations, the beating will include also polarization modulation. Its harmonicity time τ_{bh} can also be obtained from Eq. (3) by evaluating it for any polarization component containing the contributions of the waves with different central frequencies. The normalized intensity correlation function $m(\tau) = M(\tau)/M(0)$, such that $m(0) = 1$ and $m(\tau \rightarrow \infty) = 0$ [see Fig. 2(a)], is

$$m(\tau) = \frac{\langle I(t)I(t + \tau) \rangle - \langle I(t) \rangle^2}{\langle I^2(t) \rangle - \langle I(t) \rangle^2}. \quad (4)$$

It is seen that $m(\tau)$ can be measured by measuring the intensity correlation functions. For fields obeying Gaussian statistics, the function $M(\tau)$ is proportional to $|G(\tau)|^2$, where $G(\tau) = \langle E^*(t)E(t + \tau) \rangle$, with asterisk denoting the complex conjugate, is the complex temporal coherence function [1,4].

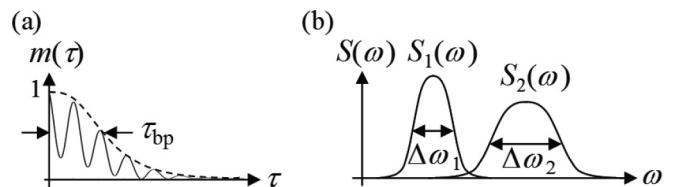


FIG. 2. (a) Normalized intensity correlation function $m(\tau)$ and the beating predictability time τ_{bh} . (b) Spectra $S_1(\omega)$ and $S_2(\omega)$ of the interfering waves.

The normalized function $m(\tau)$ can therefore be written in terms of a normalized coherence function $g(\tau) = G(\tau)/G(0)$ as $m(\tau) = |g(\tau)|^2$.

We assume, for now, that the interfering waves are independent. If the intensity spectra $S_1(\omega)$ and $S_2(\omega)$ of the waves are known, we can use the Wiener-Khinchine theorem [1,4] to find

$$g(\tau) = A \int_{-\infty}^{+\infty} [S_1(\omega) + S_2(\omega)] e^{i\omega\tau} d\omega, \quad (5)$$

where A is a constant. The spectra are shown schematically in Fig. 2(b). Taking the spectra to be Gaussian with peak values S_{0j} and spectral widths $\Delta\omega_j$, i.e.,

$$S_j(\omega) = S_{0j} e^{-\ln 2 (\omega - \omega_j)^2 / (\Delta\omega_j/2)^2}, \quad j = \{1, 2\}, \quad (6)$$

we obtain

$$m(\tau) = \frac{|\sum_{j=1,2} S_{0j} \Delta\omega_j e^{-(\Delta\omega_j\tau)^2 / (16 \ln 2) + i\omega_j\tau}|^2}{(\sum_{j=1,2} S_{0j} \Delta\omega_j)^2}. \quad (7)$$

This is a decreasing function of τ which, however, may oscillate. Requiring that the peak values of the oscillating $m(\tau)$ (or its envelope function) drop below 0.5 at τ_{bh} , we find

$$\tau_{bh} \approx \frac{2(I_1 + I_2)}{I_1 \Delta\omega_1 + I_2 \Delta\omega_2}, \quad (8)$$

where $I_j = S_{0j} \Delta\omega_j$. This approximate expression determines $1/\tau_{bh}$ as a power-weighted average of the contributions $\Delta\omega_j/2$ of the individual interfering fields. The factor of 2 in the numerator replaces $4\sqrt{\ln 2 \ln \sqrt{2}} \approx 2.0$. The beating harmonicity time thus depends directly on the spectra of the interfering independent waves.

If the separation of the central frequencies of the waves, $\Delta\omega$, is small compared to $\Delta\omega_1 + \Delta\omega_2$, then, even when $I_1 = I_2$, the beating is washed out by randomness. This is explained by the fact that the beating harmonicity time, τ_{bh} , is short compared to the beating period T_b . Notice that when one of the spectra is very narrow, say $\Delta\omega_1 \ll \Delta\omega_2$, and $I_1 = I_2$ holds, the harmonicity time is on the order of the coherence time of the beam with broader spectrum, $\tau_{bh} = 4/\Delta\omega_2$.

We point out that Eqs. (4)–(6) are not valid, if the interfering waves are not independent. As an example, let us consider interference of a wave with its coherently frequency-shifted version, e.g., obtained via the Doppler effect [27]. It can be readily verified, by decomposing the waves into their frequency components, that the frequency-shifted version of a polychromatic field $E_1(t)$ is simply equal to $CE_1(t)e^{i\Delta\omega t}$, where C is a constant. Therefore, the instantaneous intensity of the total field is

$$|E(t)|^2 = (1 + C)|E_1(t)|^2(1 + \cos \Delta\omega t), \quad (9)$$

even if the frequency shift is small compared to the fields' bandwidths. The instants of time at which the intensity maxima arrive are now fully predictable and $\tau_{bh} \rightarrow \infty$. However, the phase of the field within the intensity beats is still unpredictable after a time interval exceeding the field coherence time. We emphasize that, independent of mutual correlations of the interfering fields, Eq. (3) is valid and can be used to measure τ_{bh} .

IV. POLARIZATION BEATING OF INDEPENDENT POLYCHROMATIC WAVES

The polarization beating phenomenon can be described in terms of the Jones vectors or the Poincaré vectors [28]. The instantaneous electric-field vectors \mathbf{E}_1 and \mathbf{E}_2 of the interfering waves produce the total field $\mathbf{E} = \mathbf{E}_1 + \mathbf{E}_2$. Here and from now on we assume that the beams are independent. The corresponding instantaneous Jones vectors \mathbf{J}_1 , \mathbf{J}_2 , and $\mathbf{J} = \mathbf{J}_1 + \mathbf{J}_2$ can be obtained by dividing the considered field vectors by the same harmonically oscillating factor, such as $e^{i\omega_1 t}$. In this case, the Jones vector $\mathbf{J}_2 = \mathbf{E}_2/e^{i\omega_1 t}$ has a factor $e^{i\Delta\omega t}$. It is often difficult to obtain a clear intuitive picture of the polarization state from the form of the complex-valued Jones vector. We therefore introduce also the real-valued Poincaré vector, $\mathbf{S} = (S_1, S_2, S_3)$, whose orientation in the Poincaré space unambiguously corresponds to a certain polarization state of the field [28]. The length S_0 of the vector (the field intensity) and its three vector components are given by the following, well-known instantaneous Stokes parameters:

$$S_0 = |E_x|^2 + |E_y|^2, \quad (10)$$

$$S_1 = |E_x|^2 - |E_y|^2, \quad (11)$$

$$S_2 = 2 \operatorname{Re}\{E_x^* E_y\}, \quad (12)$$

$$S_3 = 2 \operatorname{Im}\{E_x^* E_y\}, \quad (13)$$

where E_x and E_y are any two orthogonal vector components of the total field \mathbf{E} . If the interfering fields have different polarizations, but are monochromatic or mutually correlated, the unit-length Poincaré vector, $\mathbf{s} = \mathbf{S}/S_0$, draws a circular trajectory on the surface of the Poincaré sphere [see Fig. 3(a)]. This fact has been verified by both analytical [27] and numerical calculations using Eqs. (10)–(13). It can also be understood intuitively, especially in simple cases. For example, if the interfering waves have orthogonal circular polarizations and equal intensities, the total field is linearly polarized with

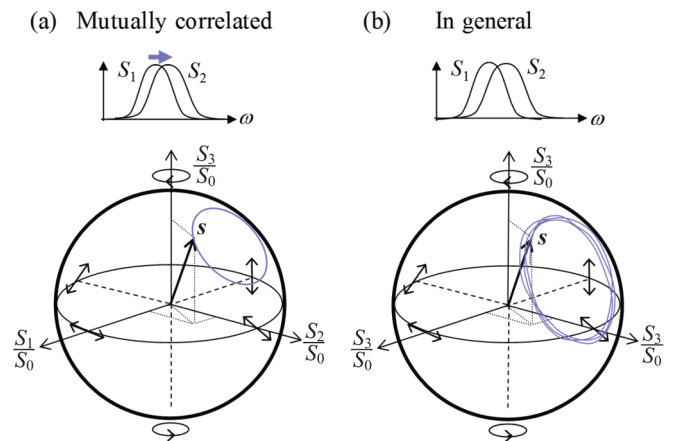


FIG. 3. Polarization beating on a unit Poincaré sphere. (a) The normalized Poincaré vector, as a function of time, draws a circular trajectory when the interfering fields are fully correlated. The thick blue arrow indicates that the spectrum S_2 is obtained from S_1 by frequency shifting. (b) If the correlation is not complete, the trajectories are randomized.

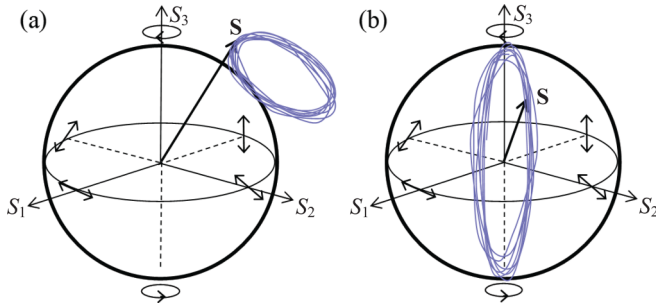


FIG. 4. Polarization beating in terms of an unnormalized Poincaré vector. Any initial polarization beating, such as that in (a), can be manipulated to make the polarization torus circular, vertical, and centered at the origin, as shown in (b).

a rotating polarization direction. The polarization beating trajectory is then the equator of the Poincaré sphere. If the intensities of the components are not equal, the circle shifts from the center, but its orientation remains unchanged. In general, the fields can be partially correlated or uncorrelated leading to randomized Poincaré-vector trajectories, as shown in Fig. 3(b).

If the polarization states of the interfering waves are not mutually orthogonal, both polarization and intensity beatings are present, and the behavior of the field must be treated in terms of the unnormalized Poincaré vector \mathbf{S} . Figure 4(a) shows schematically the general behavior of \mathbf{S} . The polarization trajectories, shown by the blue line, form on average a certain stretched “torus” with a finite thickness. The torus is not aligned with the surface of the Poincaré sphere, because when the polarizations are not orthogonal, the length of the total Poincaré vector changes in each rotation cycle. At the instances of time, at which the interfering waves are out of phase, the Poincaré vector is shortest, and it is longest when the waves are in phase.

The oscillation of the Poincaré vector can be fast. For example, a period of less than 100 fs results already from a 10-nm-wavelength difference between the interfering components in the visible spectral range. This makes the characterization of the polarization beating through measuring the instantaneous Stokes parameters difficult, if not impossible.

V. CHARACTERIZATION OF POLARIZATION BEATING IN TERMS OF TIME-AVERAGED QUANTITIES

In this section, we show that the position and orientation of the polarization-beating torus can be determined by making the interfering components have orthogonal linear polarizations and equal intensities rendering the field unpolarized. The torus of the unpolarized field turns out to be circular and have vertical orientation [see Fig. 4(b)]. In order to explain the method, let us assume that originally the waves are linearly polarized and have arbitrary amplitudes and oscillation directions. The process consists of two steps. First, the orientation angle (α) of the most intense linear-polarization component of the superposition field can be determined using a rotatable linear polarizer. At this angle, the transmittance of the polarizer is at maximum. Second, the extra power is removed from this component by a tunable partial polarizer that, ideally, does not

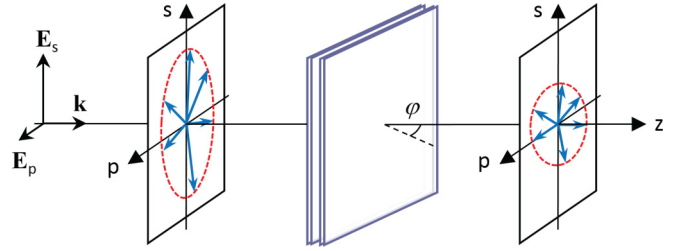


FIG. 5. Tunable partial polarizer made of two parallel glass plates. The plates are tilted by an angle φ with respect to the optical axis z . The angle φ can be adjusted such that a partially polarized wave transmitted by the plates becomes unpolarized, as the plates remove more energy from the s -polarized component than from the p -polarized one. If φ is equal to the Brewster angle, the p component is transmitted without loss.

change the power of the orthogonal polarization component. Note that both interfering waves can be present in each of these components. The procedure makes the field unpolarized. The required tunable polarizer can be constructed of tilted parallel glass plates (see Fig. 5). The ratio of the amplitude transmission coefficients of the s - and p -polarized waves of just two such plates, $\eta = (T_s/T_p)^2$, decreases by a factor of 2 when the tilt angle φ increases from 0° to 70° , as follows from the Fresnel transmittances T_s and T_p at a glass-air interface. The transmission (Jones) matrix of the device is [4]

$$\hat{\mathbf{T}}_p = \begin{pmatrix} \eta & 0 \\ 0 & 1 \end{pmatrix}, \quad (14)$$

where the initially stronger s -polarized component is assumed to be directed along the x axis.

Figure 6 illustrates an example of a deterministically beating field that is to be unpolarized as described. All the curves in the figure are obtained numerically. The original trajectories drawn by the individual electric field vectors of the waves are shown in Fig. 6(a), and Fig. 6(b) shows the trajectory (blue line) drawn by the end of the total electric-field vector within a single beating period. The frequencies of the waves are chosen such that $\Delta\omega/\omega_{av} = 0.1$ and $\omega_{av} = (\omega_1 + \omega_2)/2$. The Poincaré ellipse—drawn by the end of the total Poincaré vector—and the individual Poincaré vectors of the interfering waves, \mathbf{S}_+ and \mathbf{S}_- , are shown in Fig. 6(c). The ellipse is not centered at the origin of the coordinate system, because both the polarization and intensity beatings are present. Furthermore, the polarizations separated in time by half of the beating period are not orthogonal. The tilt angle α of the superposition-field linear polarization component with the highest intensity takes a small negative value in the present case. Letting next the field through a partial linear polarizer (as in Fig. 5) removes the extra power from this component and makes the field unpolarized. The area where the electric field oscillates becomes square shaped, as shown in Fig. 6(d), and the Poincaré ellipse becomes a vertically oriented circle centered at the origin [see Fig. 6(e)]. Note that, in spite of the fact that the field is unpolarized, it is fully deterministic.

The relative amplitude transmission coefficient of the partial polarizer η , the angle α , and the orientation angle θ of the final polarization directions of the interfering

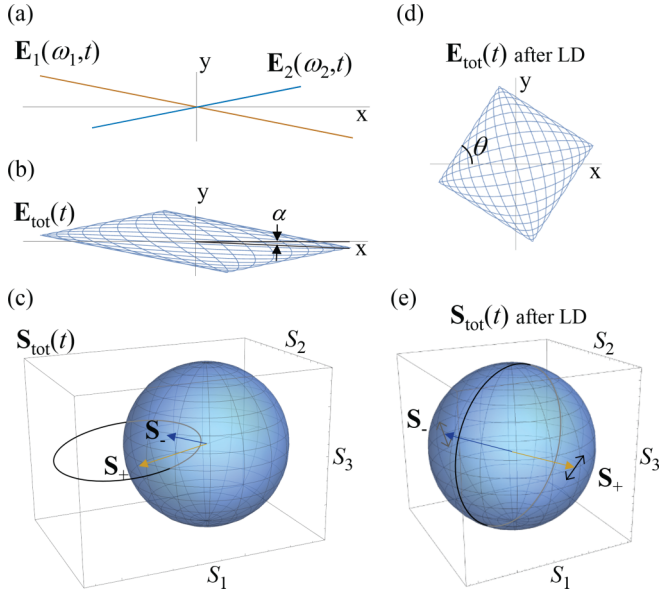


FIG. 6. Interference of two linearly polarized waves and a modification of the Poincaré ellipse. The electric-field vectors of the waves, $\mathbf{E}_1(\omega_1, t)$ and $\mathbf{E}_2(\omega_2, t)$, are shown in (a). The line drawn by the end of the total electric field vector $\mathbf{E}_{\text{tot}}(t)$ within a single beating period is shown in (b). The original Poincaré ellipse, drawn by $\mathbf{S}_{\text{tot}}(t)$, is shown in (c). Plots (d) and (e) show $\mathbf{E}_{\text{tot}}(t)$ and the trajectory of $\mathbf{S}_{\text{tot}}(t)$, respectively, after letting the field through a linear depolarizer (LD). \mathbf{S}_+ and \mathbf{S}_- are the Poincaré vectors of the interfering linearly polarized waves.

components [as shown in Fig. 6(d)] fully characterize the original polarization-beating state and the original Poincaré ellipse, as will be explained shortly. The polarization-direction angle θ can be found by transmitting the field through a rotatable linear polarizer and finding the angle (θ) at which the intensity beating is absent, indicating the presence of one frequency only. This can be done by measuring the intensity correlation functions, e.g., with the help of a Michelson interferometer and a two-photon-absorption detector [14,20]. When α , θ , and η are determined, the original polarization states and the amplitudes of the two interfering fields are found by backtransforming their final Jones vectors

$$\mathbf{J}'_1 = A \begin{pmatrix} \sin \theta \\ -\cos \theta \end{pmatrix}, \quad \mathbf{J}'_2 = A \begin{pmatrix} \cos \theta \\ \sin \theta \end{pmatrix}, \quad (15)$$

where A is a constant. The original Jones vectors are given by

$$\mathbf{J}_j = \hat{\mathbf{R}}(-\alpha) \hat{\mathbf{T}}_p^{-1} \hat{\mathbf{R}}(\alpha) \mathbf{J}'_j, \quad j = \{1, 2\}. \quad (16)$$

The coordinate rotation matrix, used to rotate the original coordinate system back to the one in which the transmission matrix $\hat{\mathbf{T}}_p$ is defined is [4]

$$\hat{\mathbf{R}}(\alpha) = \begin{pmatrix} \cos \alpha & \sin \alpha \\ -\sin \alpha & \cos \alpha \end{pmatrix}. \quad (17)$$

When the orientations and relative amplitudes of the original electric-field vectors are known, the mean trajectory of the Poincaré vector is determined using Eqs. (10)–(13).

Interestingly, if the phases of the fields \mathbf{E}_1 and \mathbf{E}_2 fluctuate, but the amplitudes are constant, the shape and orientation of

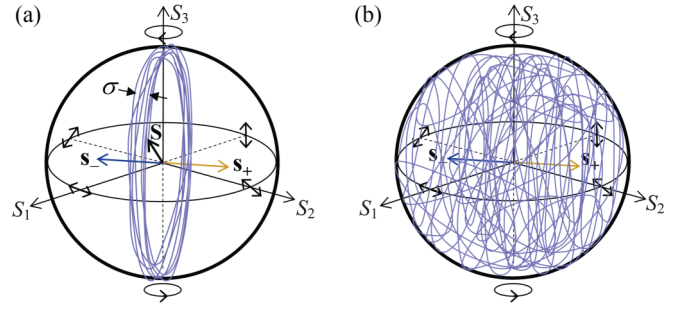


FIG. 7. Effective thickness σ of the modified Poincaré torus is shown in (a); \mathbf{s}_+ and \mathbf{s}_- are unit vectors perpendicular to the central line of the torus. In (b), the torus thickness is at its maximum, i.e., $\sigma = 1$. If the waves are fully mutually correlated, the torus is infinitely thin and $\sigma = 0$.

the Poincaré ellipse does not change in time, and only the rotation speed of the Poincaré vector changes. Indeed, the points forming the ellipse correspond to the possible instantaneous polarization states that are unambiguously defined by the amplitudes and the polarization states of the interfering waves. For example, the ellipse is fixed in time if the interfering fields are produced by intensity-stabilized single-mode lasers, *even if the lasers are independent*. If, on the other hand, the fields fluctuate in intensity, the Poincaré ellipse fluctuates in its position, shape, and orientation, but on average it is still an ellipse that, after depolarizing the field, becomes a vertically oriented circle, as in Fig. 4(b).

If the polarizations of the interfering waves are not linear, but arbitrary elliptical, one more measurement is needed. The augmented procedure is described in Appendix. At the end of the procedure, the polarizations of the interfering waves are also linear and orthogonal, and the torus is oriented vertically.

We remark that other methods to determine the geometry of the polarization torus by manipulating the polarization states and intensities of the interfering fields are possible to develop. For example, the final two orthogonal polarizations of the interfering fields can be elliptical instead of linear; note that two orthogonal linear polarizations can be made elliptical, and vice versa, by transmitting the fields through a quarter-wave plate.

VI. EFFECTIVE THICKNESS OF THE POINCARÉ TORUS

When the polarization-beating torus is circular and centered at the origin of the Poincaré sphere, one can define its effective thickness σ [see Fig. 7(a)] that is a measure of *randomness of the polarization beating*. We define σ as a normalized rms value of the projection of the instantaneous Poincaré vector on the direction \mathbf{s}_+ perpendicular to the torus, i.e.,

$$\begin{aligned} \sigma &= \sqrt{3 \frac{\langle (\mathbf{S} \cdot \mathbf{s}_+)^2 \rangle}{\langle S_0^2 \rangle}} = \sqrt{3 \frac{\langle (I_+ - I_-)^2 \rangle}{\langle (I_+ + I_-)^2 \rangle}} \\ &= \sqrt{3 \frac{\langle I_+^2 \rangle + \langle I_-^2 \rangle - 2\langle I_+ I_- \rangle}{\langle I_+^2 \rangle + \langle I_-^2 \rangle + 2\langle I_+ I_- \rangle}}. \end{aligned} \quad (18)$$

The second equality is explained by the fact that the magnitude of the Poincaré vector component along an arbitrary direction \mathbf{a} is given by the (Stokes) parameter $S_{\mathbf{a}} = I_{\mathbf{a}} - I_{-\mathbf{a}}$, where $-\mathbf{a}$ denotes the polarization state orthogonal to that related to \mathbf{a} . The direction \mathbf{s}_+ corresponds to a linear polarization of one of the interfering components. The quantity I_+ is the intensity of the field component with this linear polarization and I_- is that of the orthogonally polarized component. Their average values are $\langle I_+ \rangle = \langle I_- \rangle$. Equation (18) implies that, to measure σ , one has to measure three intensity correlation functions $\langle I_+^2 \rangle$, $\langle I_-^2 \rangle$, and $\langle I_+ I_- \rangle$ that are time-averaged quantities. The quantity σ is normalized (factor 3) such that, for fields obeying Gaussian statistics, we obtain $\sigma = 0$ if the interfering fields fully correlate, because then $\langle I_+ I_- \rangle = \langle I_+^2 \rangle = \langle I_-^2 \rangle$. If the fields are independent, we have $\sigma = 1$, because then $\langle I_+ I_- \rangle = \langle I_+ \rangle \langle I_- \rangle = \langle I_+ \rangle^2$ and $\langle I_+^2 \rangle = \langle I_-^2 \rangle = 2\langle I_+ \rangle^2$. In the latter case, the thickness of the torus is at its maximum, implying that all possible orientations of the Poincaré vector are equally probable. This situation is illustrated in Fig. 7(b).

It is of interest to consider interfering fields that have different statistics, which must be reflected in the thickness of the polarization-beating torus. For example, if one of the beams, being produced by a single-frequency laser, obeys the Poissonian statistics and the other one is still of a Gaussian statistics, the torus thickness σ is equal to $\sqrt{3/5}$, even though the interfering fields are statistically independent.

VII. CONCLUSIONS

We considered interference of polychromatic optical waves that have different central frequencies and polarizations. Such waves can have well separated spectra and exhibit ultrafast (fs-scale) polarization and intensity beatings with deterministic and random temporal variations. We introduced a characteristic time of essentially periodic polarization and/or intensity beating—that is the beating harmonicity time—and (1) calculated it in terms of the spectral intensities of the beating fields and (2) proposed a way to measure it through measuring time-averaged intensity correlation functions. We also introduced the concept of Poincaré torus that characterizes the statistical properties of polarization beating, and proposed a way to determine its orientation and thickness in terms of time-averaged quantities that can be measured using slow photodetectors.

The proposed approach to characterize the polarization and intensity beating phenomena in the general case of polychromatic waves opens up new possibilities to study and use coherence and polarization properties of light. We anticipate that further theoretical and experimental developments concerning this topic will bring about new knowledge on statistical properties of random optical fields and their new applications.

ACKNOWLEDGMENTS

Funding from the Academy of Finland (Projects No. 308394 and No. 320166) is gratefully acknowledged.

APPENDIX: CHARACTERIZATION OF POLARIZATION BEATING OF TWO ARBITRARILY ELLIPTICALLY POLARIZED WAVES

If the interfering waves have elliptical polarizations, it is still possible to determine the beating character. The measurement procedure described in Sec. V will lead to a partially polarized field in this case, and therefore an additional measurement is needed. In this measurement, the field after the second step of the previous procedure is let through a rotatable quarter-wave plate that is set to an angle β , at which an additional polarization analyzer, when rotated, shows maximum intensity modulation. Let γ be the angle of maximum transmission by the analyzer. Then, as before, the analyzer is replaced with a partial polarizer at the same angle γ to reduce the maximum intensity and make the field unpolarized. The Poincaré ellipse will after this step be a vertical circle, similar to the one obtained above in Fig. 6(e). The procedure makes the interfering waves, on average, linearly polarized, orthogonal, and equal in amplitudes. The original polarization states of the interfering waves can be found by backtransforming the final average Jones vectors \mathbf{J}'_j , $j = \{1, 2\}$, using the transmission matrices of the involved optical

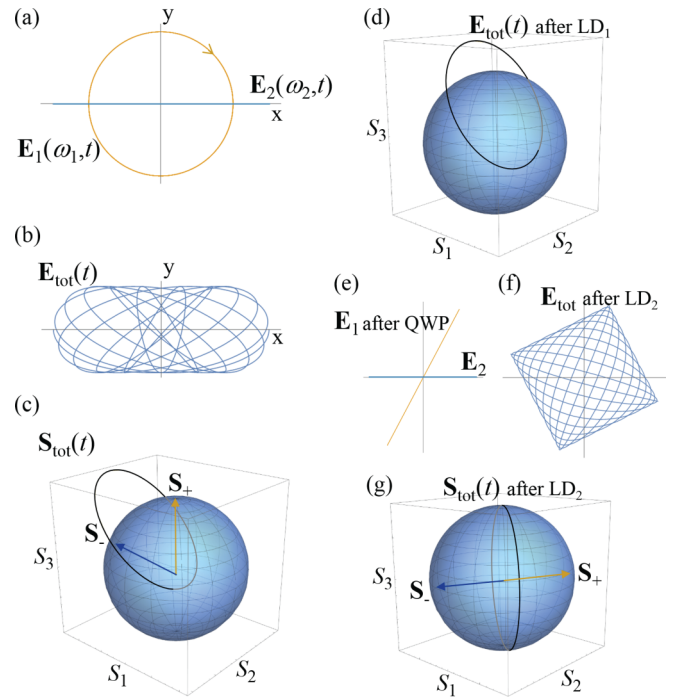


FIG. 8. Interference of a circularly and a linearly polarized wave and a modification of the Poincaré ellipse. The electric-field vectors of the waves are $\mathbf{E}_1(\omega_1, t)$ and $\mathbf{E}_2(\omega_2, t)$, as shown in (a). The line drawn by the end of the total electric-field vector $\mathbf{E}_{\text{tot}}(t)$ within a single beating period is shown in (b). The original Poincaré ellipse, drawn by $\mathbf{S}_{\text{tot}}(t)$, is shown in (c). Plot (d) shows the trajectory of $\mathbf{S}_{\text{tot}}(t)$ after letting the field through a linear depolarizer (LD_1). The fields $\mathbf{E}_1(t)$ and $\mathbf{E}_2(t)$ after applying a quarter-wave plate (QWP) are shown in (e). Plots (f) and (g) show $\mathbf{E}_{\text{tot}}(t)$ and the trajectory of $\mathbf{S}_{\text{tot}}(t)$, respectively, after applying a linear depolarizer again. \mathbf{S}_+ and \mathbf{S}_- are the Poincaré vectors of the interfering waves.

elements, i.e.,

$$\mathbf{J}_j = \hat{\mathbf{R}}(-\alpha)\hat{\mathbf{T}}_p^{-1}\hat{\mathbf{R}}(\alpha)\hat{\mathbf{R}}(-\beta)\hat{\mathbf{G}}^{-1}\hat{\mathbf{R}}(\beta)\hat{\mathbf{R}}(-\gamma)\hat{\mathbf{T}}_p^{-1}\hat{\mathbf{R}}(\gamma)\mathbf{J}'_j, \quad (\text{A1})$$

where the transmission matrix of the quarter-wave plate is [4]

$$\hat{\mathbf{G}} = \begin{pmatrix} 1 & 0 \\ 0 & -i \end{pmatrix}. \quad (\text{A2})$$

The mean trajectory of the Poincaré vector is then obtained by using Eqs. (10)–(13).

As an example, let us consider interference of a linearly polarized wave and a circularly polarized one of different frequency. Figures 8(a) and 8(b) show the original polarization states of the two components and the trajectory

of the total electric-field vector, respectively. The original Poincaré ellipse is shown in Fig. 8(c). After applying a partial linear polarizer that reduces the intensity of the x -polarized components (LD_1), the Poincaré ellipse is shifted such that the S_3 axis crosses its center [see Fig. 8(d)]. Indeed, since now any two orthogonal linear polarization components of the field are equally strong, the projection of the ellipse on the (S_1, S_2) plane is symmetric with respect to the origin. After the quarter-wave plate, the two interfering fields become linearly polarized [see Fig. 8(e) for the polarizations of these fields], and after the second partial polarizer (LD_2), the polarizations become orthogonal [see Fig. 8(f) for the behavior of the total field]. Figure 8(g) shows the final, vertical, Poincaré circle.

-
- [1] L. Mandel and E. Wolf, *Optical Coherence and Quantum Optics* (Cambridge University Press, Cambridge, UK, 1995).
 - [2] K. Kokkonen and M. Kaivola, *Appl. Phys. Lett.* **92**, 063502 (2008).
 - [3] B. P. Abbott *et al.*, *Phys. Rev. Lett.* **116**, 061102 (2016).
 - [4] B. E. A. Saleh and M. C. Teich, *Fundamentals of Photonics* (John Wiley & Sons, New York, 2007).
 - [5] K. Kikuchi, *J. Light. Technol.* **34**, 157 (2016).
 - [6] S. Hooker and C. Webb, *Laser Physics* (Oxford University Press, Oxford, 2010).
 - [7] A. Shevchenko, P. Ryytty, T. Kajava, M. Hautakorpi, and M. Kaivola, *Appl. Phys. B* **74**, 349 (2002).
 - [8] A. F. Fercher, W. Drexler, C. K. Hitzenberger, and T. Lasser, *Rep. Prog. Phys.* **66**, 239 (2003).
 - [9] B. I. Erkmen and J. H. Shapiro, *Adv. Opt. Photon.* **2**, 405 (2010).
 - [10] J. Rosen, B. Katz, and G. Brooker, *3D Res.* **1**, 28 (2010).
 - [11] W. Demtröder, *Laser Spectroscopy: Basic Concepts and Instrumentation* (Springer, Berlin, 2003).
 - [12] A. A. Mikhailovsky, M. A. Petruska, M. I. Stockman, and V. I. Klimov, *Opt. Lett.* **28**, 1686 (2003).
 - [13] K. G. Gåsvik, *Optical Metrology* (John Wiley & Sons, New York, 2002).
 - [14] A. Shevchenko, M. Roussey, A. T. Friberg, and T. Setälä, *Optica* **1**, 64 (2017).
 - [15] E. Pisanty, G. J. Machado, V. Vicuña-Hernández, A. Picón, A. Celi, J. P. Torres, and M. Lewenstein, *Nat. Photon.* **13**, 569 (2019).
 - [16] D. Sugic and M. R. Dennis, *J. Opt. Soc. Am. A* **35**, 1987 (2018).
 - [17] F. Maucher, S. Skupin, S. A. Gardiner, and I. G. Hughes, *Phys. Rev. Lett.* **120**, 163903 (2018).
 - [18] F. Maucher, S. Skupin, S. A. Gardiner, and I. G. Hughes, *New J. Phys.* **21**, 013032 (2019).
 - [19] T. Bauer, P. Banzer, E. Karimi, S. Orlov, A. Rubano, L. Marrucci, E. Santamato, R. W. Boyd, and G. Leuch, *Science* **347**, 964 (2015).
 - [20] F. Boitier, A. Godard, E. Rosencher, and C. Fabre, *Nat. Phys.* **5**, 267 (2009).
 - [21] G. J. Verbiest and M. J. Rost, *Nat. Commun.* **6**, 6444 (2015).
 - [22] J. M. Coupland, *Top. Appl. Phys.* **77**, 373 (2000).
 - [23] J. Eichholz, D. B. Tanner, and G. Mueller, *Phys. Rev. D* **92**, 022004 (2015).
 - [24] C. Greiner, B. Boggs, T. Wang, and T. M. Mossberg, *Opt. Lett.* **23**, 1280 (1998).
 - [25] H. Lajunen, J. Salaj, and T. Setälä, *J. Eur. Opt. Soc.-Rapid* **11**, 16011 (2016).
 - [26] A. Shevchenko, M. Roussey, A. T. Friberg, and T. Setälä, *Opt. Express* **23**, 31274 (2015).
 - [27] A. Hannonen, K. Saastamoinen, L.-P. Leppänen, M. Koivurova, A. Shevchenko, A. T. Friberg, and T. Setälä, *New J. Phys.* **21**, 083030 (2019).
 - [28] C. Brosseau, *Fundamentals of Polarized Light: A Statistical Optics Approach* (Wiley, New York, 1998).